Regimes of feedback-controlled beam coupling

B. Sturman and E. Podivilov
International Institute for Nonlinear Studies, Institute of Automation and Electrometry, Russian Academy of Sciences, Koptyug Avenue 1, 630090 Novosibirsk, Russia

M. Gorkunov
Institute of Crystallography, Russian Academy of Sciences, Leninskii pr. 59, 117333 Moscow, Russia
(Received 29 January 2005; published 20 July 2005)

The introduction of certain electronic feedback loops into photorefractive wave-coupling schemes makes them noise free and leads to dramatic changes of the whole nonlinear behavior. The familiar steady states can be transformed into periodic states that are characterized by ultimately high and low values of the diffraction efficiency η of the recorded index grating or into quasisteady states with small values of η. These transformations possess thresholds with respect to controllable experimental parameters like the coupling strength and the input intensity ratio. We present a general analysis of the threshold behavior for different modes of the feedback operation and different types of the nonlinear photorefractive response. The results obtained (analytical and numerical) allow one to predict the regions of stability for feedback-controlled steady states and the observable characteristics of the system, including the output amplitudes and diffraction efficiency of the spatial grating, beyond these regions. They extend strongly the potentialities of the feedback-controlled wave coupling.

DOI: 10.1103/PhysRevE.72.016621 PACS number(s): 42.40.Pa, 42.70.Nq, 42.65.Sf, 42.65.Hw

I. INTRODUCTION

Two-wave coupling owing to photorefractive (PR) nonlinearity is well understood nowadays both theoretically and experimentally [1–3]. The incident light beams (with fixed input intensities and phases) record a refractive index grating (via light-induced charge separation and the linear electro-optic effect) and experience mutual Bragg diffraction from this spatial grating. As a result, a steady state is achieved; this state is characterized by the energy and phase exchange between the interacting beams and also by the spatial modulation of the index grating. Such a steady state is unique, and the diffraction efficiency of the recorded dynamic grating ranges between 0 and 1. Quantitative characteristics of the steady states depend on the type and strength of the photorefractive nonlinear response—i.e., on the phase shift between the index and light fringes and on how large the grating amplitude is at a given value of light contrast.

Implementation of a certain feedback loop, whose function is to adjust the phase φ_s of one of the incident beams (let it be signal beam S) depending on the output intensity of this beam (see Fig. 1), brings us to a qualitatively new dynamic nonlinear system which has no close analogs among the known nonlinear devices. Mathematically, the novelty of this system is due to the nonlinearity and nonlocality of the boundary conditions expressing the feedback equations. Physically, the possibility for implementation of various electronic feedbacks between the optical input and output is caused by the specific feature of the PR nonlinearity—its relative slowness.

Initially the feedback in question was implemented to stabilize the input light fringes [4,5]. It was found later that this feedback changes strongly the observable properties of beam coupling and grating recording in sufficiently thick photorefractive $LiNbO_3$ crystals [6–9]. In particular, it has led to a 100% diffraction efficiency η of the recorded grating and suppressed the harmful effect of nonlinear light scattering. The first experimental publications included also an important idea about the principle of the feedback operation. It has been postulated that the input phase φ_s is adjusted in such a way so as to make equal $\pm\pi/2$ the phase difference Φ_s between the diffracted and transmitted components of the S beam.

Numerical modeling of the feedback-controlled beam coupling in $LiNbO_3$ crystals has shown [10] that the imposition of the ideal feedback condition $\Phi_s=\pm\pi/2$ enforces the system to approach quickly a state with $\eta=1$ or 0 if the crystal thickness d is sufficiently large. At this state, however, the transmitted or diffracted component of the S beam turns to zero so that the phase difference Φ_s becomes unde-

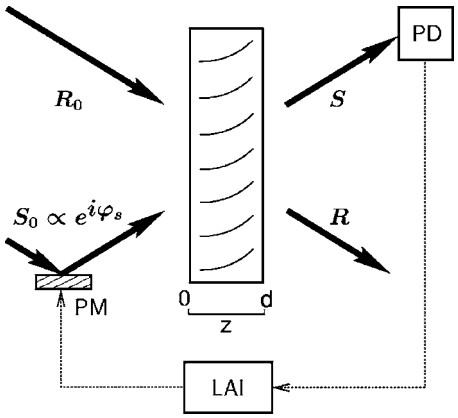

FIG. 1. Schematic of a feedback-controlled two-wave coupling experiment; PD is a photodiode, LAI is a lock-in amplifier and integrator, and PM is a piezomirror. The bent lines show schematically the grating fringes.

fined. In other words, the postulated ideal conditions $\Phi_s(\varphi_s)=\pm\pi/2$ are valid only within a restricted time interval; they lose their meaning for $\eta\simeq 1$ or 0 and cannot explain the permanent operation of the system.

Further analysis of the feedback operation has allowed to modify the ideal feedback conditions by taking into account a weak inertia of the electronic feedback loop [11,12]. An inertial feedback condition, represented by a dynamic nonlinear equation for the input phase φ_s, ensures a permanent operation mode. On the other hand, it is not much different from the corresponding ideal condition unless $\eta\simeq 1$ or 0. It is useful therefore to specify different feedback conditions by indicating the ideal values of Φ_s; see also below.

Employment of the inertial feedback conditions $\pm\pi/2$ for simulation of the feedback-controlled wave coupling in $LiNbO_3$ crystals has allowed one to predict the crossover from familiar steady states to periodic states (attractors) with increasing crystal thickness d and other critical parameters like the input light contrast [11,12]. These periodic states are distinguished by small oscillations of η in the close vicinity of 1 or 0, strong oscillations of φ_s, and the presence of a frequency detuning Ω between the light beams. Distinct periodic states possess different values of Ω, different oscillation periods, and different shapes of the phase modulation. All predicted periodic states are found experimentally in lithium niobate crystals [11,12].

The use of numerical and analytical methods has allowed during the last years to extend and refine our knowledge of the capabilities of the new nonlinear-optical device [13–17]. However, a number of fundamental and practically important questions about the feedback operation still remain unanswered.

(i) Construction of the electronic feedback loop admits, as known, not only the $\pm\pi/2$ feedback conditions (ideal or inertial) but also the 0, π conditions; see Sec. II C for more details. What is the impact of the last-named feedbacks on the observable characteristics of two-wave coupling?

(ii) How the impact of different feedbacks depends on the type of the nonlinear response?

(iii) The major control parameters in the feedback experiments are the input intensity ratio r_0 and the coupling strength $|\Gamma_0|d$ (the mathematical definitions are given below). What are the regions on the r_0, $|\Gamma_0|d$ plane with qualitatively different feedback behavior?

The main purpose of this paper is to answer these questions. It is important that the lines separating different regions of the r_0, $|\Gamma_0|d$ plane (the separatrices) can be found on the basis of simple analytical considerations. They give, in particular, the regions of stability of the familiar steady states—i.e., define the threshold for the appearance of new dynamic regimes that are not necessarily periodic states. Direct numerical simulations are needed within this approach to qualify the type of dynamic regime. In short, we are going to classify different nonlinear regimes and different possibilities for the feedback operation on the basis of general analytical considerations.

II. BASIC RELATIONS

A. Coupled-wave and material equations

In the case of photorefractive nonlinearity, the refractive index change is due to formation of the space-charge field and the linear electro-optic effect [1,2]. In accordance with Fig. 1, we present the space-charge field as $E_{sc}=(1/2)E\exp(iKx)+\text{c.c.}$, where K is the grating vector and $E=E(z,t)$ is the complex slowly varying grating amplitude. The index change is given by $\delta n=-rn^3E_{sc}/2$, where r is the relevant electro-optic coefficient and n is the background refractive index.

The coupled-wave equations for the light amplitudes S and R, which describe Bragg diffraction from the grating, are given by [1,2]

$$\frac{\partial R}{\partial z}=i\kappa ES,\quad \frac{\partial S}{\partial z}=i\kappa E^*R, \tag{1}$$

where $\kappa=\pi n^3r/\lambda$ is the known real coefficient and the asterisk means complex conjugation. The total light intensity is a conserving quantity within the set (1). For convenience we normalize the light amplitudes in such a way that $|R|^2+|S|^2=1$.

The grating amplitude E obeys a material equation that accounts for the processes of charge separation under light. In what follows we restrict ourselves to the following fairly general model equation [2,3]:

$$\left(t_r\frac{\partial}{\partial t}+1\right)E=2F\,RS^*, \tag{2}$$

where t_r is the PR response time (inversely proportional to the total intensity) and F is a complex coefficient characterizing the PR nonlinearity. The absolute value of the product $2RS^*$ is the light contrast m.

In steady state with R and S being time independent (standing light pattern) we have $E=2F\,RS^*$. The absolute value $|F|$ is here the coefficient of proportionality between $|E|$ and m while $\Psi=\arg F$ is the spatial phase shift between the index and light fringes. The limiting cases of real and imaginary F ($\Psi=0,\pi$ and $\pm\pi/2$) correspond to the so-called local and nonlocal PR response, respectively. The local response is usually due to the drift of photoexcited charge carriers and/or the bulk photovoltaic effect. The nonlocal response is often due to diffusion of the charge carriers.

In the literature one can find numerous model relations expressing F and t_r through the applied electric field E_0, the grating vector K, and material parameters; see, e.g., [2] and references therein. For many PR ferroelectrics ($LiNbO_3$, $LiTaO_3$, $BaTiO_3$, $KNbO_3$, etc.) it is sufficient to suppose that t_r is the dielectric relaxation time, $F=E_{pv}-E_0\mp iE_D$, where E_{pv} is the photovoltaic field, $E_D=Kk_bT/e$ is the diffusion field, k_b is the Boltzmann constant, T is the absolute temperature, and e is the elementary charge. The upper and lower signs correspond to the photoexcitation of electrons and holes, respectively.

B. Fundamental amplitudes

Since the problem of Bragg diffraction is linear, we can represent the amplitudes S and R as linear combinations of the transmitted (first) and diffracted (second) components (see also [10,12,18,19]),

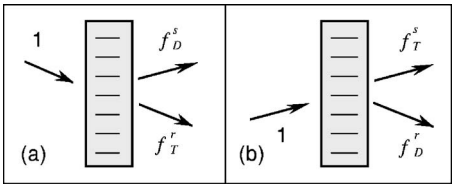

FIG. 2. Geometrical schemes relevant to the definition of the fundamental amplitudes.

$$S = S_0 f_T^s + R_0 f_D^s, \quad R = R_0 f_T^r + S_0 f_D^r, \tag{3}$$

where $R_0 = R(0,t)$ and $S_0 = S(0,t)$ are the input amplitudes. The fundamental amplitudes $f_T^r(z,t)$ and $f_D^s(z,t)$ correspond to testing of the grating by a unit R beam; see Fig. 2(a). They meet the same coupled-wave equations as R and S, respectively; the boundary conditions for them are $f_T^r(0,t)=1$, $f_D^s(0,t)=0$. The fundamental amplitudes $f_D^r(z,t)$ and $f_T^s(z,t)$ correspond to testing of the same grating by a unit S beam; see Fig. 2(b). Their input values are 0 and 1, respectively. The amplitudes $f_{T,D}^r$ and $f_{T,D}^s$ fully describe the transmission and diffraction properties of the dynamic grating.

At the first sight, Eqs. (3) are useless because we cannot express four fundamental amplitudes by two amplitudes S and R. However, by making the complex conjugation of the coupled-wave equations for f_T^r and f_D^s one can see easily that

$$f_T^s = f_T^{r*}, \quad f_D^s = -f_D^{r*}. \tag{4}$$

Only two fundamental amplitudes (let them be f_T^s and f_D^s) are independent thus owing to the symmetry properties of the coupled-wave equations. Using Eqs. (3) and (4), we express f_T^s and f_D^s explicitly through the recording amplitudes,

$$f_T^s = S_0^* S + R_0 R^*, \quad f_D^s = R_0^* S - S_0 R^*. \tag{5}$$

Some other properties of the fundamental amplitudes are important as well. In accordance with our definitions [see also Fig. 2 and Eqs. (4)], we have $\eta = |f_D^s(d)|^2 = |f_D^r(d)|^2$. These relations prove that the result of measurements of η does not depend on which of the recording beams (R or S) is blocked. They allow one to express η explicitly through the recording amplitudes. Furthermore, we have $|f_T^s(d)|^2 = |f_T^r(d)|^2 = 1-\eta$. Last, we mention that the equality $\eta = 1$ ensures the relation $r_d = r_0^{-1}$ between the output ($r_d = |S_d|^2/|R_d|^2$) and input ($r_0 = |S_0|^2/|R_0|^2$) intensity ratios (the intensity interchange).

Using Eqs. (3) and (4) we express now the phase difference Φ_s between the diffracted and transmitted components of the S beam through the input and output characteristics of the recording beams,

$$\Phi_s = \varphi_r - \varphi_s + \arg[(S_0 S_d^* + R_0^* R_d)(R_0^* S_d - S_0 R_d^*)], \tag{6}$$

where $R_d = R(d,t)$ and $S_d = S(d,t)$ are the output values of the recording amplitudes and $\varphi_s = \arg S_0$ and $\varphi_r = \arg R_0$ are the input phases of the S and R beams. Note that relation (6) is general; it is free of any particular assumptions about properties of the PR response.

C. Feedback conditions

In experiment, the adjustment of the input phase φ_s is accomplished with the help of a modulation technique [4,6]. An auxiliary oscillating component $\delta\varphi_s = \psi_d \sin \omega t$, whose amplitude ψ_d and period $2\pi/\omega$ are much smaller than 1 and the PR response time t_r, respectively, is introduced into φ_s. This component does not affect the grating and serves for operation of the electronic feedback loop.

To describe the influence of the auxiliary phase modulation on the amplitude S, it is sufficient to replace S_0 by $S_0 \exp(i\psi_d \sin \omega t)$ in the first of Eqs. (3). Then, using the smallness of ψ_d and the above relations for the fundamental amplitudes, one can make sure that the output intensity $|S_d|^2$ acquires high-frequency components oscillating as $\sin \omega t$ and $\cos 2\omega t$. Their amplitudes are

$$I_\omega = m_0 \sqrt{\eta(1-\eta)}\,\psi_d \sin \Phi_s,$$

$$I_{2\omega} = (m_0/4)\sqrt{\eta(1-\eta)}\,\psi_d^2 \cos \Phi_s, \tag{7}$$

where $m_0 = 2|S_0 R_0^*|$ is the input light contrast. The amplitudes I_ω and $I_{2\omega}$ are generally functions of time; they are expected to vary slowly as compared to $\sin \omega t$. Both expressions include the phase difference Φ_s.

Further steps of the feedback operation can be commented with the help of Fig. 1. The photodetector (PD) transforms linearly the output intensity $|S_d|^2(t)$ into an electric-voltage signal. This signal is filtered using the heterodyne principle and the components $I_\omega(t)$ and $I_{2\omega}(t)$ are extracted. Last, they arrive at a lock-in amplifier and integrator (LAI). One of the amplified and integrated signals drives a piezomirror (PM).

Since the PM displacement is proportional to the driving voltage, the time derivative of the input phase $\dot{\varphi}_s$ is proportional to I_ω or $I_{2\omega}$. Supposing for definiteness that the integrated $I_{2\omega}$ signal is chosen to govern the input phase, we arrive at the feedback equation [11,12]

$$\dot{\varphi}_s = \mp \frac{m_0}{t_f}\sqrt{\eta(1-\eta)} \cos \Phi_s, \tag{8}$$

where t_f is a new time constant determined by the LAI and PM specifications (see [6] and references therein for details of the electronics). It will be referred to as the feedback loop response time. The feedback inertia is weak when $t_f \ll t_r$; this case is indeed of our prime interest. Note the possibility of choice between the signs + and − in the feedback equation. As we shall see, the operation modes for the signs + and − are different. The feedback equation which is relevant to the use of I_ω signal is obtained by the replacement of $\cos \Phi_s$ by $\sin \Phi_s$ in Eq. (8). Generally speaking, any linear combination of the signals I_ω and $I_{2\omega}$ can be used to govern the feedback loop [8].

Consider now the relationship between the derived inertial feedback equations and the ideal feedback conditions. To understand it, we recall that (i) the diffraction properties of the grating are changing on the scale of the PR response time t_r (i.e., very slowly on the scale of t_f) and (ii) the phase Φ_s is the difference between the feedback governed input phase φ_s and a quantity that also varies slowly on the scale of t_f; see Eq. (6). According to Eq. (8), the phase Φ_s relaxes then to

$\pm\pi/2$ on the time scale of t_f unless the product $\eta(1-\eta)$ is close to zero; i.e., the inertial feedback equations are almost equivalent here to the ideal feedback conditions $\Phi_s=\pm\pi/2$. If we use $\pm I_\omega$ as the error signal in the feedback loop, the phase Φ_s arrives quickly to the ideal values $0,\pi$ unless $\eta=0,1$. It is sufficient thus to indicate the ideal value of Φ_s to specify the corresponding inertial feedback condition. In the general case, by making use of combinations of I_ω and $I_{2\omega}$, one can access the inertial feedback with an arbitrary ideal value of Φ_s.

A direct experimental proof of correctness of the feedback equation (8) is presented in [20]. The ratio t_f/t_r was estimated as $\approx 10^{-3}$ for experiments with lithium niobate crystals. This estimate was used in the previous numerical simulations on the feedback-controlled beam coupling [11,12]. It will be used also in the subsequent numerical calculations.

III. FEEDBACK-CONTROLLED STEADY STATES

A. General relations

In the general case, a frequency detuning Ω exists between the R and S beams in steady state so that the light and index fringes are moving with a constant velocity Ω/K. We attribute this detuning to the linear change of the input phase $\varphi_s(t)$. We set $S\propto\exp(-i\Omega t)$ and $E\propto\exp(i\Omega t)$ to take it into account. Equations (1) and (2) give then the known relations for the wave amplitudes,

$$R=R_0\exp(\Gamma z/2)/D,\quad S^*=S_0^*\exp(-\Gamma z/2)/D, \tag{9}$$

where the denominator $D=D(z)$ is given by

$$D=[|R_0|^2\exp(\Gamma' z)+|S_0|^2\exp(-\Gamma' z)]^{\Gamma/2\Gamma'} \tag{10}$$

and $\Gamma=\Gamma'+i\Gamma''$ is the complex rate constant,

$$\Gamma=i\Gamma_0/(1+i\Omega t_r)\ \text{with}\ \Gamma_0=2\kappa F. \tag{11}$$

Its real part Γ' is referred to as the amplitude gain factor; the imaginary part Γ'' characterizes the phase coupling.

Using Eqs. (5) and (9), one can find the following explicit relations for the fundamental amplitudes:

$$f_T^s=[|R_0|^2\exp(\Gamma^* z/2)+|S_0|^2\exp(-\Gamma^* z/2)]/D^*,$$

$$f_D^s=-R_0^*S_0[\exp(\Gamma^* z/2)-\exp(-\Gamma^* z/2)]/D^*. \tag{12}$$

Since $\eta=|f_D^s(d)|^2$, we obtain, for steady-state diffraction efficiency,

$$\eta=\frac{m_0^2}{2}\frac{\cosh(\Gamma' d)-\cos(\Gamma'' d)}{\cosh(\Gamma' d)+W_0\sinh(\Gamma' d)}, \tag{13}$$

where $W_0=|R_0|^2-|S_0|^2=(r_0-1)/(r_0+1)$ is the normalized input intensity difference and $r_0=|R_0|^2/|S_0|^2$ is the input intensity ratio. This relation incorporates the coupling effects; it is equivalent to an expression known since 1979 [21].

Let us maximize and minimize η as a function of the coupling parameters $\Gamma' d$ and $\Gamma'' d$. The maximum value of the efficiency is $\eta_{max}=1$. The maximizing value of $\Gamma'' d$ meets the equation $\cos(\Gamma'' d)=-1$—i.e., $\Gamma'' d=\pm\pi,\pm 3\pi,\ldots$. The maximizing value of $\Gamma' d$ is unique; it is given by relation $\tanh(\Gamma' d/2)=-W_0$. The minimum value $\eta_{min}=0$ is achieved when $\Gamma'=0$ and $\Gamma'' d=\pm 2\pi,\pm 4\pi,\ldots$. *Two conditions* have to be satisfied thus to turn η to 1 (or to 0). The reason is simple: The value $\eta=1$ (or 0) is achieved when both real and imaginary parts of $f_T^s(d)$ [or $f_D^s(d)$] are zeros.

The derived conditions will play an important role in the subsequent analysis. The condition $\eta=1$ (or 0) gives us a sequence of branches for the coupling strength $|\Gamma_0|d$ as a function of r_0—i.e., a sequence of curves on the $|\Gamma_0|d, r_0$ plane. These curves, as we will see, separate the regions with different feedback-controlled behavior. They will be referred to as the *separatrices* or *threshold curves*. Each point of a separatrix corresponds to a unique value of the frequency detuning, i.e., $\Omega=\Omega(r_0)$.

Next, using Eqs. (6) and (12), we calculate the steady-state phase difference Φ_s,

$$\Phi_s=\arg[W_0\cos(\Gamma'' d)+i\sin(\Gamma'' d)-\sinh(\Gamma' d)-W_0\cosh(\Gamma' d)]. \tag{14}$$

It is well defined unless $\eta(1-\eta)=0$. The lines $\eta(|\Gamma_0|d, r_0)=1$ and 0 serve thus as boundaries of the regions where the phase difference Φ_s is well defined.

The feedback is able to adjust the steady-state value of Φ_s by varying the detuning Ω. Consider the main possibilities, which are relevant to different choices for the real and imaginary parts of the complex quantity inside the square brackets in Eq. (14).

(i) $\Phi_s=\pm\pi/2$. It is equivalent to the following two conditions:

$$\sinh(\Gamma' d)+W_0\cosh(\Gamma' d)=W_0\cos(\Gamma'' d),$$

$$\sin(\Gamma'' d)\gtrless 0. \tag{15}$$

(ii) $\Phi_s=0,\pi$. In this case we have

$$\Gamma'' d=j\pi,$$

$$\sinh(\Gamma' d)+W_0\cosh(\Gamma' d)\lesseqgtr W_0(-1)^j, \tag{16}$$

where $j=0,\pm 1,\ldots$.

Each of these relations specifies some regions on the $|\Gamma_0|d, r_0$ plane. If we replace in Eqs. (15) and (16) the sign $\gtrless$ by the sign $=$, we obtain a set of curves that separate the regions where steady-state solutions with $\Phi_s=\pi/2$ and $-\pi/2$ [or $\Phi_s=0$ and π] take place. Different separatrices and regions look fairly simple when we restrict ourselves to not very large values of the coupling strength $|\Gamma_0|d$. Below we consider a number of important particular cases.

B. Separatrices: Particular cases

The local response. Here we set first, see Eq. (11), $\Gamma_0=|\Gamma_0|$ to obtain

$$\Gamma'=\frac{|\Gamma_0|\Omega t_r}{1+\Omega^2 t_r^2},\quad \Gamma''=\frac{|\Gamma_0|}{1+\Omega^2 t_r^2}. \tag{17}$$

With $\Omega=0$ the rate coefficient Γ is pure imaginary.

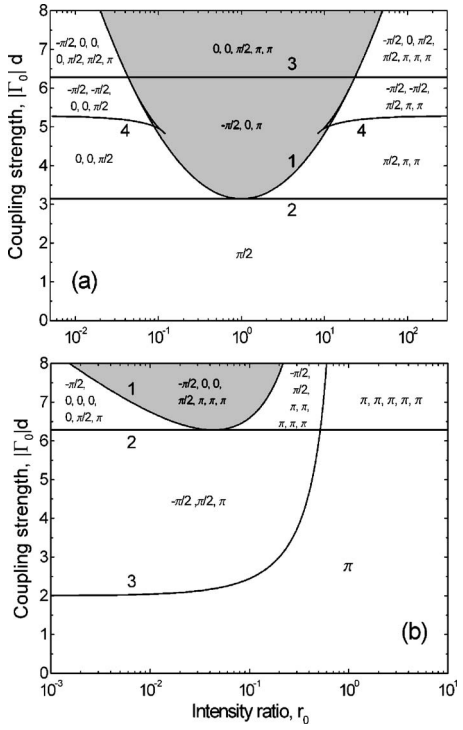

FIG. 3. Lines separating different regions on the $r_0, |\Gamma_0|d$ plane for the local (a) and nonlocal (b) responses. Separatrix 1 corresponds to the condition $\eta=1$; above it (within the gray regions) periodic states take place. The signs $0, \pi/2, \ldots$ mean that steady-state solutions with $\Phi_s=0, \pi/2, \ldots$ can be found formally within the indicated regions. Repetition of the same sign means the frequency degeneration—two, three, … steady states with the same value of Φ_s but different values of Ω correspond to one pair r_0, $|\Gamma_0|d$.

The condition $\eta=1$ is fulfilled when

$$|\Gamma_0|d = j\pi + \frac{1}{j\pi}\ln^2 r_0, \tag{18}$$

with $j=1,3,\ldots$. Separatrix 1 in Fig. 3(a) shows the coupling strength $|\Gamma_0|d$ versus the input intensity ratio $r_0=|R_0|^2/|S_0|^2$ for $j=1$ (the branches with $j=3,5,\ldots$ correspond to much higher values of $|\Gamma_0|d$). This dependence is symmetric to the replacement r_0 by r_0^{-1}. The minimum value of the coupling strength, $(|\Gamma_0|d)_{min}=\pi$, takes place at $r_0=1$. The detuning relevant to the condition $\eta=1$ is given by $\Omega t_r=-\ln r_0/\pi$; it changes sign when r_0 is replaced by r_0^{-1}. The condition $\eta=0$ is fulfilled when $\Omega=0$ and $|\Gamma_0|d=2\pi, 4\pi, \ldots$; see line 3 in Fig. 3(a).

Consider now the lines separating the regions with different steady-state values of Φ_s. Two additional separatrices 2 and 4 are necessary to specify different regions for $|\Gamma_0|d<3\pi$; see Fig. 3(a). Below line 2—i.e., for $|\Gamma_0|d<\pi$—the only possible steady state corresponds to $\Phi_s=\pi/2$. Two additional states with $\Phi_s=0$ (or with $\Phi_s=\pi$) can formally be found within the region restricted by the curves 1, 2, and 4. The number of possible steady states—i.e., the number of solutions of Eqs. (15) and (16)—grows with increasing $|\Gamma_0|d$. Keeping this fact in mind, it is easy to understand that intersection of lines 1 and 3 [they correspond to the conditions $\eta(|\Gamma_0|d, r_0)=1$ and 0, respectively] does not contradict common sense because these lines separate different branches of steady-state solutions.

To make more use of Fig. 3(a), we consider a representative example. Imagine that we increase $|\Gamma_0|d$ starting from 0 for $r_0=10^2$. Crossing line 2 results in the appearance of two steady-state solutions with $\Phi_s=\pi$ but it does not affect the solution with $\Phi_s=\pi/2$. Crossing line 4 is not accompanied by qualitative changes with respect to the steady states with $\Phi_s=\pi/2$ and π; it results, however, in the appearance of two new solutions with $\Phi_s=-\pi/2$. Crossing line 3, where $\eta=0$, is accompanied by a bifurcation for all types of steady states; in particular, the unique $\pi/2$ branch splits into two branches. Note, last, that crossing separatrix 1, where $\eta=1$, also results in a bifurcation for all branches of steady-state solutions.

For each admitted type of steady-state solution ($\Phi_s=-\pi/2, 0, +\pi/2, \pi$) the frequency detuning Ω is a function of r_0 and $|\Gamma_0|d$. When several solutions of the same type are allowed, each point of the $r_0, |\Gamma_0|d$ plane corresponds to several values of Ω.

We will see below that most of the feedback-controlled steady states are unstable for large values of $|\Gamma_0|d$; such states cannot be realized in practice and they are of minor interest.

What happens if the sign of the local response is inverted, $\Gamma_0=-|\Gamma_0|$? The answer is simple: Within all above regions, the feedback sign (and the sign of Ω) has to be inverted to ensure the same behavior of the system. The form of separatrix 1 remains unchanged.

The nonlocal response. Here we set first $\Gamma_0=-i|\Gamma_0|$ which gives the relations

$$\Gamma' = \frac{|\Gamma_0|}{1+\Omega^2 t_r^2}, \quad \Gamma'' = -\frac{|\Gamma_0|\Omega t_r}{1+\Omega^2 t_r^2}. \tag{19}$$

The rate coefficient Γ is real for $\Omega=0$ and the energy transfer $S\to R$ takes place.

The condition $\eta=1$ is fulfilled when

$$|\Gamma_0|d = -(\ln r_0 + \pi^2/\ln r_0). \tag{20}$$

This relation describes the lowest branch of the dependence of $|\Gamma_0|d$ on r_0; see separatrix 1 in Fig. 3(b). The allowed values of r_0 are smaller than 1 so that the contrast m is an increasing function of the propagation coordinate z. The absolute minimum of the coupling strength, $(|\Gamma_0|d)_{min}=2\pi$, is 2 times higher than that for the local response; it occurs at $r_0=\exp(-\pi)\simeq 0.043$. The relevant dependence $\Omega(r_0)$ is given by $\Omega t_r=\pi/\ln r_0$; the optimizing value of Ωt_r is -1.

Apart from separatrix 1, lines 2 and 3 shown in Fig. 3(b) are important to describe possible steady-state solutions. For sufficiently small values of the coupling strength the only possible state corresponds to the condition $\Phi_s=\pi$. Two additional steady-state solutions with $\Phi_s=\pm\pi/2$ appear in the region restricted by the lines 2 and 3. For $|\Gamma_0|d>2\pi$ there are at least four different regions. For each of them one can find several different feedback-controlled steady states. Most of them are not stable. Each type of the feedback-controlled steady state corresponds, as earlier, to a separate branch of the dependence $\Omega(r_0, |\Gamma_0|d)$.

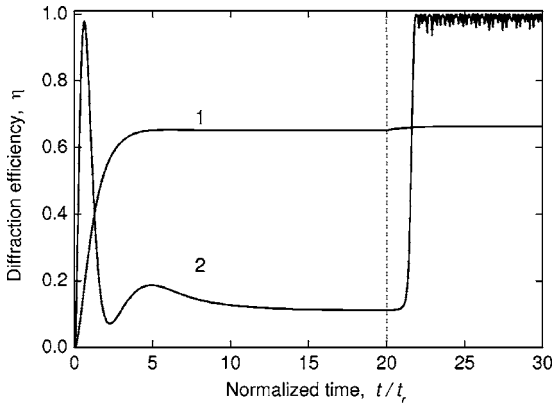

FIG. 4. Dependences $\eta(t)$ for the case of the local response, $r_0=2$, and two different values of the coupling strength. The curves 1 and 2 are plotted for $|\Gamma_0|d=2$ and 7, respectively. The moment when the $\pi/2$ feedback is switched on, $t=20t_r$, is shown by the vertical dashed line. For $t<20t_r$ the time evolution occurs under fixed input parameters. The region of curve 2 where $\eta\simeq 1$ corresponds to a periodic state.

What happens if the sign of the nonlocal response is inverted, $\Gamma_0=i|\Gamma_0|$—i.e., if the direction of the energy transfer is $R\rightarrow S$? Separatrix 1 in Fig. 3(b) is replaced by the mirror-reflected curve; i.e., the allowed values of r_0 are larger than 1.

C. Stable and unstable feedback-controlled steady states

By speaking of stability of the found steady states we mean stability against small perturbations: Imagine that a small perturbation is superimposed on a steady state. If this perturbation is decreasing in time, the state is stable; if it is increasing, the state is unstable.

It is worth mentioning that each steady state refers not only to the feedback-controlled system (with proper boundary conditions imposed on the opposite crystal faces) but also to the conventional PR system with certain prescribed input values R_0 and S_0. However, the properties of stability of these two systems are entirely different. In the second case, all steady states are stable, whereas in the first case there are stable and unstable steady-state solutions.

The problem of stability is very resistent to analytical studies. It can, however, be solved numerically. To clarify the essence of our analysis, we describe two representative numerical experiments; see also [10]. For both of them, the nonlinear response is local, $\Gamma_0=|\Gamma_0|$, the feedback is initially switched off, and some input values $R_0(t)=\text{const}$ and $S_0(t)\propto\exp(-i\Omega t)$ are imposed. The input intensity ratio $r_0=|R_0|^2/|S_0|^2$ is the same in both experiments but the values of $|\Gamma_0|d$ and Ω are different: For the first try, the above three parameters are chosen in such a way that $\Phi_s\simeq\pi/2$ in steady state and the point $\log r_0, |\Gamma_0|d$ lies below separatrix 2 in Fig. 3(a). For the second try, the point $\log r_0, |\Gamma_0|d$ lies above separatrix 3 and again $\Phi_s\simeq\pi/2$ in steady state.

With the feedback switched off and the input parameters fixed, the conventional system always arrives at a unique steady state. The initial sections of curves 1 and 2 in Fig. 4 (they are to the left of the dashed line) exhibit the corresponding dependences of $\eta(t)$ for the transient process with a zero initial value of the grating amplitude. This shows that the steady state with $\Phi_s=\pi/2$ is stable for the conventional system and ensures small perturbations of the amplitudes.

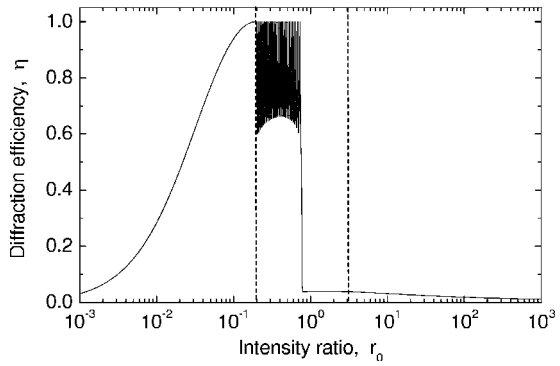

FIG. 5. Dependence $\eta(r_0)$ for the case of local response $\Gamma_0 d=4$, the inertial $(t_f/t_r=10^{-3})$ feedback condition $\Phi_s=0$, and the input beam ratio r_0 slowly increasing from 10^{-3} to 10^3; the vertical dashed lines mark the boundaries of the gray region at the chosen value of the coupling strength.

At $t=20t_r$ the feedback $\pi/2$ is switched on; i.e., instead of the boundary conditions at the input we have imposed proper boundary conditions that couple the amplitudes R and S on the opposite faces of the sample. One sees that the behavior of $\eta(t)$ does not experience any visible changes for the first numerical experiment and changes strongly for the second one. In the second case $\eta(t)$ does not tend to any steady-state value; see also below. We conclude that the second steady state is not stable.

The above described method can be improved by using an *adiabatic procedure*: We can change slowly (on the scale of the PR response time t_r) the parameters r_0 and/or $|\Gamma_0|d$ upon approaching a certain steady state. Within the region of these parameters where the feedback-controlled steady state is stable the diffraction efficiency (and/or other observable characteristics) follows adiabatically the steady-state values. As soon as the steady state becomes unstable, the efficiency shows dramatic temporal changes and deflects strongly from its steady-state value. We can find in this way the boundary of the stability region.

An example of the use of the adiabatic procedure for the case of local response $(\Gamma_0=|\Gamma_0|)$ is shown in Fig. 5.

After approaching very closely the conventional steady state, which is characterized by $\Phi_s=0$, $\Gamma_0 d=4$, and $r_0=10^{-3}$, we switched on the 0 feedback condition and increased slowly (with the rate $\approx 10^{-2}t_r^{-1}$) the beam ratio r_0 from 10^{-3} to 10^3. Until crossing separatrix 1 the diffraction efficiency η practically coincides with its steady-state value. After crossing this separatrix [i.e., within the gray region of Fig. 3(a) where the steady-state solution with $\Phi_s=0$ is allowed] the system exhibits first a nonstationary periodic behavior; the phase difference Φ_s deflects here strongly from a zero value. For $r_0\gtrsim 0.8$ (i.e., within the gray region) the diffraction efficiency drops down abruptly and remains very small with increasing r_0; the phase Φ_s is far from zero in this range (see also the next section for more details).

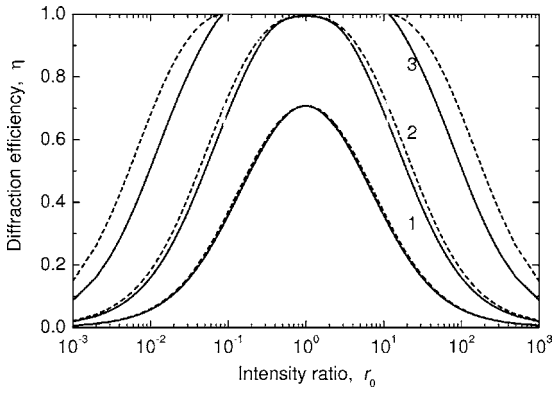

FIG. 6. Dependence $\eta(r_0)$ for the case of the local response and three different values of the coupling strength. The curves 1, 2, and 3 are plotted for $|\Gamma_0|d=2$, 3, and 5, respectively. The solid lines correspond to the condition $\Phi_s=\pi/2$ while the dashed lines are obtained by the Ω maximization of $\eta(r_0,\Gamma_0 d,\Omega)$.

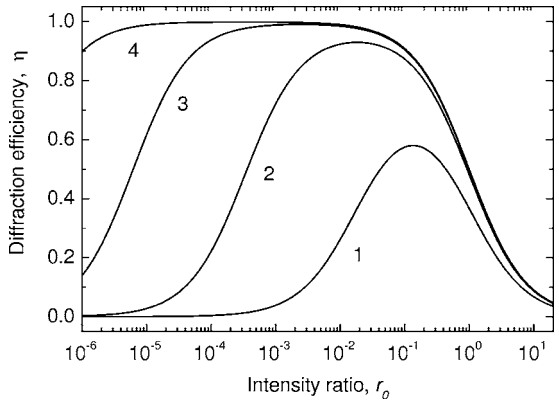

FIG. 7. Dependence $\eta(r_0)$ for the case of nonlocal local response, the feedback condition $\Phi_s=\pi$, and four values of the coupling strength. The curves 1, 2, 3, and 4 are plotted for $|\Gamma_0|d=2$, 4, and 6, and 8, respectively.

Let us summarize the results of our stability analysis. Consider first the case of local PR response, $\Gamma_0=|\Gamma_0|$. Above separatrix 1—i.e., inside the gray region in Fig. 3(a)—all formally allowed feedback-controlled steady states are not stable. For each point lying outside the gray region we always have one stable $\pi/2$ state. Below line 3 this state is unique; above this line the stable $\pi/2$ branch possesses the highest value of η. Within the left and right white regions restricted by curves 1, 2, and 4 we have additionally one stable 0 and π state, respectively. Within the left white region restricted by curves 1, 3, and 4, one of two states with $\Phi_s=0$ and one of two states with $\Phi_s=-\pi/2$ are stable. Within the right white region restricted by curves 1, 3, and 4, one of two states with $\Phi_s=\pi$ and one of two states with $\Phi_s=-\pi/2$ are stable. Within the white regions above line 3, one state with $\Phi_s=0$ and one state with $\Phi_s=\pi$ are stable in addition to the state with $\Phi_s=\pi/2$. In any case, two or more branches of the same type cannot be stable simultaneously in the case of local response.

Consider now some observable characteristics of the above stable steady states. The solid lines in Fig. 6 show the dependence $\eta(r_0)$ for the $\pi/2$ feedback and several representative values of the coupling strength $\Gamma_0 d$.

The dashed lines show the dependences $\eta(r_0)$ (for the same values of $\Gamma_0 d$) that are obtained under the condition of maximum diffraction efficiency. In other words, for each combination of $\Gamma_0 d$ and r_0 we have chosen the value of Ω maximizing η; $\Phi_s\neq\pi/2$ in this case. One sees that the $\pi/2$ feedback does not maximize $\eta(\Gamma_0 d,r_0)$ in the general case. The maximization occurs only for $r_0=1$ (when $|\Gamma_0|d<\pi$) and for the values of $\Gamma_0 d$ and r_0 belonging separatrix 1 in Fig. 3(a). At the same time, the solid and dashed lines are very close to each other for $\Gamma_0 d\lesssim\pi$; the $\pi/2$ feedback leads in this region to an almost ideal maximization of η. The higher $\Gamma_0 d$ and $|\log r_0|$, the worse is the feedback maximization. The gaps in the dependences $\eta(r_0)$ for $\Gamma_0 d>\pi$ are caused by the disappearance of the steady state with $\Phi_s=\pi/2$ in the gray region in Fig. 3(a).

Now we turn to the case of nonlocal response $\Gamma_0=-i|\Gamma_0|$. In accordance with Fig. 3(b), one branch of steady-state solutions relevant to the condition $\Phi_s=\pi$ exists in the whole range of parameters $|\Gamma_0|d$ and r_0; this branch is distinguished by a zero value of the frequency detuning, $\Omega=0$. This important solution is stable everywhere, including the gray region restricted by the separatrix 1. All other steady-state solutions that are allowed in the gray region are not stable.

Outside the gray region the allowed steady states with $\Phi_s=\pm\pi/2$ are stable. Two of four additional states with $\Phi_s=\pi$, which exist above the line 2, are stable as well. The same is true with regard to two of four states with $\Phi_s=0$ that are allowed above line 2. In such a way, we have the situation when two or even three stable steady states are possible under the same external conditions. The result of the feedback-controlled evolution depends here on the initial conditions for the grating amplitude.

Consider now the most remarkable features of the mentioned stable steady-state solution with $\Phi_s=\pi$ and $\Omega=0$.

Figure 7 shows the diffraction efficiency η as a function of the input beam ratio r_0 for four representative values of the coupling strength. With increasing $|\Gamma_0|d$ this function approaches closely the unit value within a wide range of r_0.

IV. NONLINEAR REGIMES

A. Main options

For any combination of the experimental parameters $|\Gamma_0|d$ and r_0 and for any type of the PR nonlinearity (local or nonlocal) one can impose any of four main feedbacks 0, $\pm\pi/2$, and π. The question now is *what are the expected regimes of the feedback operation?*

Prior to answer this fundamental question, we systematize the results of the previous analysis: It is possible that (a) the feedback admits at least one stable steady state, (b) the feedback admits unstable steady-state solutions, or (c) the feedback does not admit steady-state solutions (the "forbidden feedback").

One can expect that the nonlinear system arrives to a steady state in the case (a). This expectation, however, can fail. It is possible that a stable (against small perturbations) state is unattainable for certain initial conditions. In such

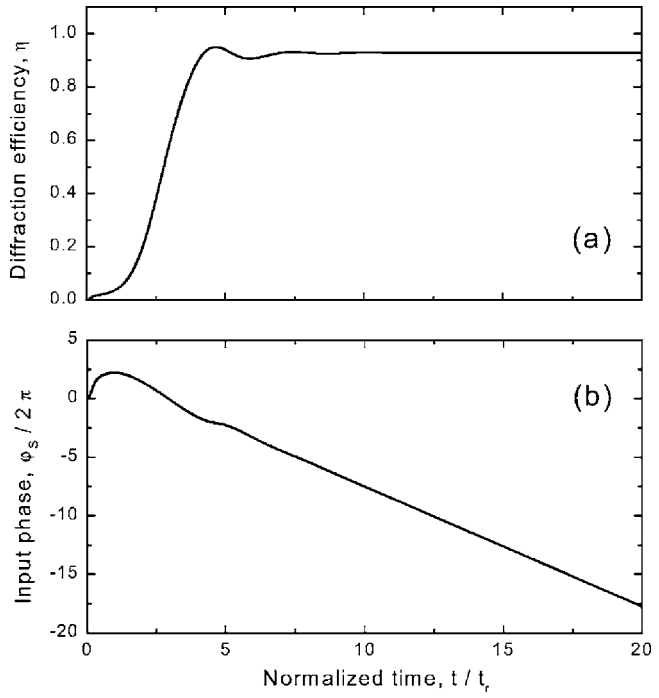

FIG. 8. Dependences $\eta(t)$ and $\varphi_s(t)$ for the feedback 0 in the case of local response $\Gamma_0 d=6.5$ and $r_0=0.01$.

cases (they occur most often near the border of the gray region) the observable characteristics of the system depend on its prehistory; the final stage of the feedback-controlled evolution can, e.g., be different when we start from zero and nonzero values of the grating amplitude. In the cases (b) and (c) one might expect essentially non-steady-state behavior of the system. Typically, this expectation is correct but in some cases it is wrong.

Our extensive numerical experiments have allowed to identify four main scenarios of the feedback-controlled evolution.

(i) *Achievement of a stable steady state*. In this case $0<\eta<1$, the phase difference Φ_s is fixed by the relevant feedback condition, and the input phase $\varphi_s(t)$ increases or decreases linearly, which means the presence of a frequency detuning Ω between the R and S beams. Typically it takes place for the variant (a); see above. The feedback inertia is not important in this case; the ideal and inertial feedback conditions give essentially the same results.

This scenario is illustrated by Fig. 8 for the local response and the feedback 0. Despite a rather large value of the coupling strength [we are above separatrix 3 in Fig. 3(a)] and proximity of the gray region, the steady state is achieved without any complicated transient stage. The diffraction efficiency approaches the steady-state value ($\simeq 0.92$) in about $t\approx 7t_r$ and the feedback-controlled input phase $\varphi_s(t)$ first experiences a growth and then decreases with a constant rate, $\Omega\simeq -6t_r^{-1}$.

(ii) *Achievement of a familiar periodic state*. This scenario is typical for the case (b). The efficiency η oscillates here in the close vicinity of 1 or 0, the phase difference $\Phi_s(t)$ shows strong oscillations, and the input phase $\varphi_s(t)$ experiences strong oscillations superimposed generally on a linear trend.

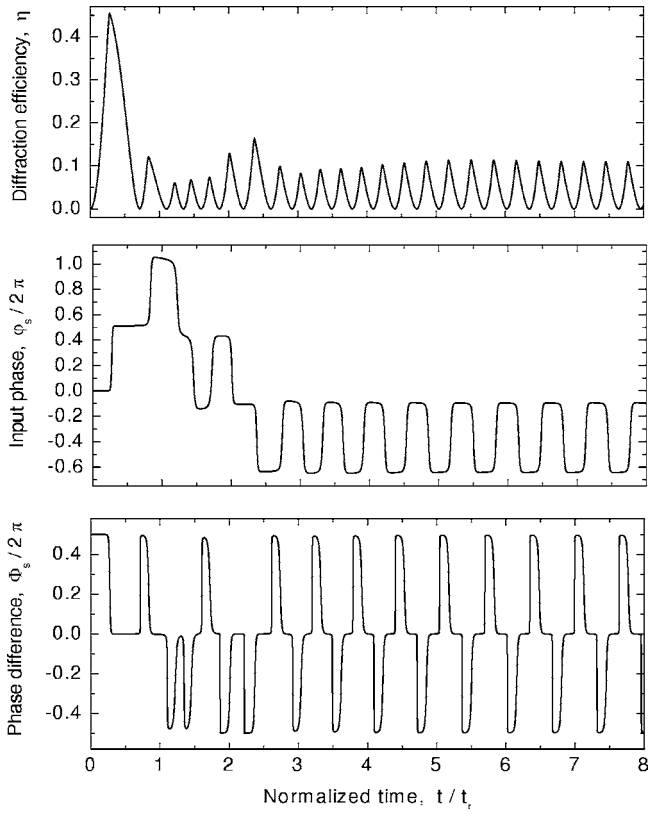

FIG. 9. Dependences $\eta(t)$, $\varphi_s(t)$, and $\Phi_s(t)$ showing the achievement of a periodic state with $\eta(t)\ll 1$ in the case of nonlocal response, $|\Gamma_0|d=8$, $r_0=0.1$, and the 0 feedback.

Inertia of the feedback loop is crucial in this case. Examples of such a periodic behavior for the local response, the $\pi/2$ feedback, $\eta(t)\simeq 1$, and $\Omega\neq 0$ are known from [11,12]; this regime is also illustrated by Fig. 4. Here we exhibit a new periodic state which is relevant to the nonlocal response $\Gamma_0=-i|\Gamma_0|$, the 0 feedback, and $\eta(t)\ll 1$; see Fig. 9.

The chosen parameters correspond to the gray region of Fig. 3(b). One sees that after a rather short transient stage the system arrives at a periodic state. It is distinguished by periodic $\simeq\pm\pi$ jumps of the input phase $\varphi_s(t)$ with a zero average slope. The phase difference $\Phi_s(t)$ deflects strongly from a zero value which is expected for the ideal fee back condition; the influence of the feedback inertia (it is characterized by the ratio $t_f/t_r=10^{-3}$) is extremely strong.

(iii) *Achievement of a quasisteady state relevant to the erasure operation mode*. This scenario occurs typically for the variant (c). The imposed feedback condition is not compatible here with the achievement of a genuine steady state. Trying to approach the forbidden value of Φ_s, the feedback establishes a very-high-frequency detuning; the value of Ω is restricted only by the feedback inertia. As a result, the space-charge grating is very weak and $\eta\ll 1$. An example of this behavior for the 0 feedback is given in Fig. 10.

The diffraction efficiency η, the frequency detuning Ω, and the phase difference Φ_s are about 27%, $12t_r^{-1}$, and 7°, respectively, at the final stage. Oscillations of the observable parameters are absent. The same mode of feedback operation can be seen in Fig. 5 for $r_0\gtrsim 0.8$.

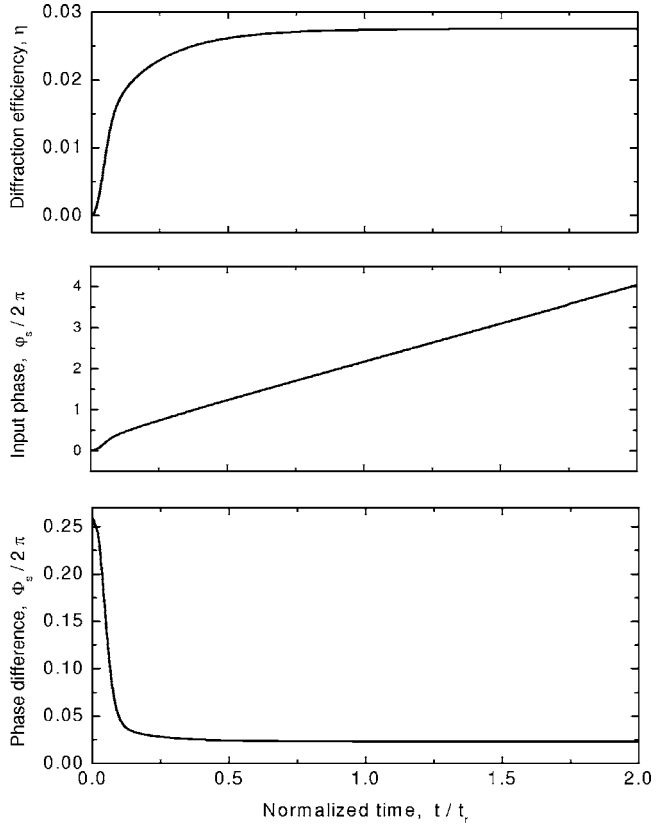

FIG. 10. Dependences $\eta(t)$, $\varphi_s(t)$, and $\Phi_s(t)$ for the local response, $\Gamma_0 d=2$, $r_0=1$, and the forbidden 0 feedback.

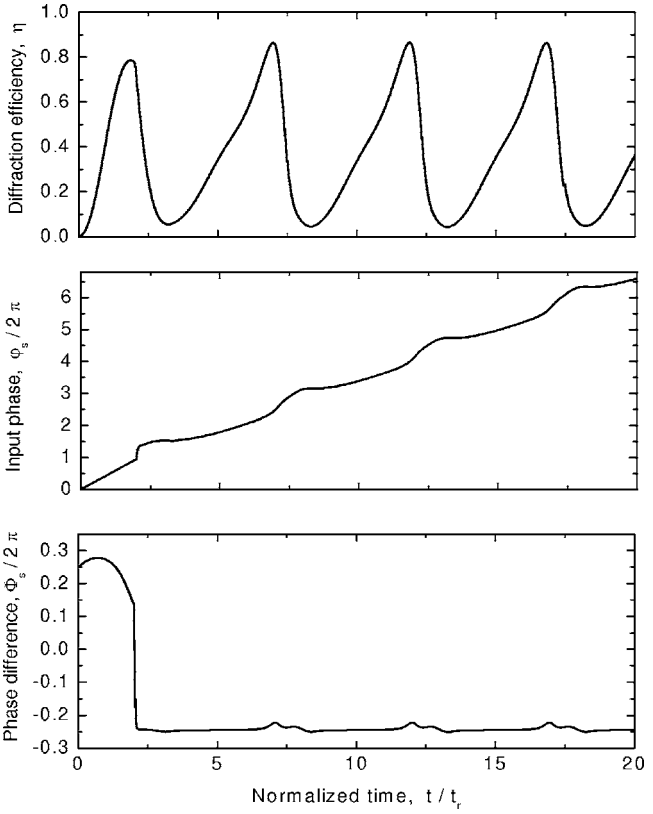

FIG. 11. Dependences $\eta(t)$, $\varphi_s(t)$, and $\Phi_s(t)$ for the local response, $\Gamma_0 d=8$, $r_0=100$, and the feedback $-\pi/2$.

(iv) *Achievement of an anomalous periodic state*. In this case, the diffraction efficiency $\eta(t)$ oscillates with a large amplitude and a large period. These characteristics are almost free of the influence of the feedback inertia. This new scenario of the feedback-controlled behavior is illustrated by Fig. 11 for the case of local response, $\Gamma_0 d=8$, and $r_0=100$.

At the final stage, the phase difference Φ_s is close to the "ideal" value $-\pi/2$ and the diffraction efficiency oscillates between $\simeq 0.04$ and 0.8 while the input phase φ_s experiences noticeable periodic oscillations and grows on average with a constant with a constant rate. Another example of the same regime can be seen in Fig. 5 for $0.2 \lesssim r_0 \lesssim 0.8$.

B. What and where can be achieved?

The purpose of this subsection is to outline what kind of nonlinear behavior is expected in different regions of the $|\Gamma_0|d, r_0$ plane for different types of the PR response and different feedback conditions.

The local response. Different regions of the $|\Gamma_0|d, r_0$ plane are given here by Fig. 3(a). Outside the gray region the use of the "allowed" $\pi/2$ feedback always results in achievement of a unique steady state with $0<\eta<1$; i.e., regime (i) takes place. Within the gray region, this feedback brings the system to a periodic state with $\eta \simeq 1$; i.e., regime (ii) occurs. The situation with other feedbacks is more complicated.

Below separatrix 2 the forbidden feedbacks $-\pi/2$, 0 and π correspond to regime (iii)—i.e., to the achievement of a quasisteady state with $|\Omega|t_r \gg 1$ and $\eta \ll 1$.

In the left white region restricted by curves 1, 2, and 4 the use of the allowed feedback 0 results usually in regime (i) and seldom in regime (iii). With the forbidden feedbacks $-\pi/2$ or π the system develops here according to regime (iii). Since crossing curve 4 does not affect steady states with $\Phi_s=0$ and π, nothing is changing for the feedbacks 0 and π in the left white region restricted by curves 1, 3, and 4. The use of the $-\pi/2$ feedback leads here to the steady state. In the left white region above separatrix 3 employment the 0 and π feedbacks typically brings the system to the corresponding steady states [regime (i)]. Near the border of gray region regime 3 also becomes possible. The feedback $-\pi/2$ leads often to anomalous periodic states [regime (iv)].

The above described with respect to the left white regions is applicable to the mirror-reflected right white regions if we replace the feedback 0 by the feedback π.

Consider now the gray region. The use of feedbacks 0 and π leads here either to periodic states with $\eta \simeq 1$ [regime (ii)] or to quasisteady states with $\eta \ll 1$ [regime (iii)]. The higher the coupling strength, the larger is the amplitude of periodic oscillations of $\eta(t)$; regime (ii) can thus transform gradually into regime (iv). For modest values of the coupling strength, $|\Gamma_0|d \lesssim 2\pi$, the feedback $-\pi/2$ leads either to periodic states with $\eta \ll 1$ or to quasisteady states. For larger values of $|\Gamma_0|d$ periodic states with large oscillations of η [regime (iv)] become possible.

The nonlocal response. Different regions of the $|\Gamma_0|d, r_0$ plane are given now by Fig. 3(b). The feedback π always leads to establishment of a stable steady state. Except for two

right white regions above line 2, this state is unique and it corresponds to $\Omega=0$. Within the mentioned white regions, one of three stable steady states is expected to be achieved. For not very large values of $|\Gamma_0|d$ these states possess similar characteristics.

The use of the forbidden $\pm\pi/2$ and 0 feedbacks in the white region restricted from above by curves 2 or 3 leads to quasisteady states with $\eta \ll 1$ [regime (iii)]. In the adjacent white region restricted from above and below by curves 2 and 3, respectively, the feedbacks $\pm\pi/2$ lead the system to the corresponding unique stable steady states [regime (i)]. The forbidden 0 feedback correspond here to periodic states with $\eta(t) \ll 1$ [regime (ii)].

Within the left white region restricted by curves 1 and 2, the $\pm\pi/2$ feedbacks also lead to establishment of steady states; the corresponding values of η can be very close to 1. The use of the feedback 0 results here either in steady states or periodic states with $\eta(t) \simeq 1$. The behavior of the system for the $\pm\pi/2$ feedbacks remains similar in the white region restricted by curves 1, 2, and 3; however, the use of 0 feedback leads here to periodic states with $\eta \ll 1$. Last, in the upper right region we have quasisteady states [regime (iii)] for all forbidden feedbacks ($\pm\pi/2$ and 0).

Within the gray region we have periodic states with $\eta(t) \simeq 1$ for the $\pm\pi/2$ feedbacks. The 0 feedback can lead to different periodic states: Near the left boarder we observed typically regime (iv) with modest and large deviations of $\eta(t)$ from 1. Near the right border of the region we have typically regime (ii) with $\eta(t) \ll 1$.

V. DISCUSSION

Let us discuss first the main merits of our theoretical approach that combines analytical and numerical tools.

We have found a simple approach to the problem of feedback-controlled wave coupling. It is based on determination of the regions of essentially different nonlinear behavior on the plane of experimental parameters, coupling strength $|\Gamma_0|d$, and the input intensity ratio r_0. The curves separating these regions (separatrices) can be found analytically for two main types of the photorefractive nonlinear response (local and nonlocal) and four main kinds of the feedback conditions ($\pm\pi/2$, 0, and π).

As soon as the separatrices are drawn, we know whether a certain feedback (and chosen experimental parameters) is compatible with the existence of steady-state solutions for the wave amplitudes. If the answer is negative (the forbidden feedback), achievement of a conventional steady state is not possible. Thus, we can obtain important information about nonlinear behavior of our nonlinear system.

If a steady-state solution is formally possible (the allowed feedback), it is either stable or nonstable against small perturbations. Fortunately, the borders of different regions on the $|\Gamma_0|d, r_0$ plane, which are obtained from the steady-state analysis, determine the borders of the stability regions. This enables us to determine, using numerical tools, which of the allowed feedback-controlled steady-state solutions are stable.

The next problem is to classify different regimes of the feedback operation and to describe when and how they can be realized. Basically, this nonlinear problem and especially its second part, is very difficult. Knowledge of the regions of the existence and stability of the feedback-controlled steady states is not sufficient for a full-scale analysis of possible nonlinear regimes. However, there is a strong correlation between the relatively simple results of our steady-state analysis and the nonlinear behavior of the feedback-controlled system. This has allowed us to present a qualitative (but not complete) picture of the expected feedback-controlled behavior for not too large values of the coupling strength.

Our analysis has extended considerably the range of expected manifestations and applications of the feedback-controlled wave coupling. Earlier the main efforts were focused on the case of local response and the feedbacks $\pm\pi/2$. The present theory has covered all main types of the PR nonlinearity and feedback conditions.

A simple and useful outcome of this generalization is the notion of allowed and forbidden feedbacks. A forbidden feedback is not compatible with steady-state solutions; switching to such an operation mode always results in erasure of the space-charge field. The use of proper allowed feedbacks leads to maximization of the diffraction efficiency for any types of PR response.

It is interesting that the periodic states that are found for different types of feedback conditions possess essentially different observable characteristics. It is possible, in particular, to realize not only the periodic states with shallow and fast oscillations of the diffraction efficiency but also the states with big and slow periodic changes.

The establishment of the familiar steady states with $\Omega=0$ for any values of the coupling strength in the case of nonlocal response and the π feedback is also an important outcome of our analysis. It means that the feedback ensures stabilization (against phase fluctuations) the conventional effects of spatial amplification and energy transfer.

In addition to the above considered cases of local and nonlocal PR nonlinearity, the case of the so-called resonant nonlinear response would be of a big interest. This response is typical for dc-biased photorefractive crystals of the sillenite family ($Bi_{12}RO_{20}$, $R=Si, Ti, Ge$) and semiconductors like GaAs and CdTe. Its distinctive feature is a considerable enhancement of the grating amplitude under the condition of the linear resonance $\Omega=\omega_K$ between the detuning Ω and the eigenfrequency of weakly damped space-charge waves ω_K; see [2,22] and references therein. The first experiments on feedback-controlled wave coupling in the case of the resonant response were performed in [23,24]. Theoretical considerations of this case are complicated by the necessity to take into account the excitation of higher spatial harmonics $(2K, 3K, \ldots)$ of the space-charge field for the values of light contrast $m \sim 1$ [22,25] and also by the vectorial character of wave coupling [26].

We hope that this theoretical study opens new prospects for experiments on feedback-controlled wave coupling in different photorefractive materials.

VI. CONCLUSIONS

For two main types of the photorefractive nonlinear response, local and nonlocal, and four different types of feed-

back conditions, $\Phi_s=0$, $\pm\pi/2$, and π, we have found analytically the regions of experimental parameters (the coupling strength and the input intensity ratio) with qualitatively different nonlinear behavior.

Using direct numerical simulations, we have identified four main nonlinear regimes for the feedback-controlled wave coupling.

(i) Achievement of a conventional steady state with moving light fringes.

(ii) Achievement of a conventional periodic states with small and fast oscillations of the diffraction efficiency near the values of 1 and 0.

(iii) Realization of a quasisteady state with an extremely large value of the frequency detuning between the recording waves and a small value of the diffraction efficiency.

(iv) Establishment of an anomalous periodic state with large and slow oscillations of the diffraction efficiency.

It is found finally how to proceed to these regimes using the notion of regions with different feedback-controlled behavior.

ACKNOWLEDGMENT

Financial support from the Russian Foundation for Fundamental Studies (Grant No. 03-02-16083) is gratefully acknowledged.

[1] *Photorefractive Materials and Their Applications I*, edited by P. Günter and J.-P. Huignard, Vol. 61 of *Topics in Applied Physics* (Springer-Verlag, Berlin, 1988).

[2] L. Solymar, D. J. Webb, and A. Grunnet-Jepsen, *The Physics and Applications of Photorefractive Materials* (Clarendon Press, Oxford, 1996).

[3] K. Buse, Appl. Phys. B: Lasers Opt. **64**, 391 (1997).

[4] A. A. Kamshilin, J. Frejlich, and L. Cescato, Appl. Opt. **25**, 2375 (1986).

[5] J. Frejlich, L. Cescato, and G. F. Mendes, Appl. Opt. **27**, 1967 (1988).

[6] A. Freschi and J. Frejlich, J. Opt. Soc. Am. B **11**, 1837 (1994).

[7] P. M. Garcia, K. Buse, D. Kip, and J. Frejlich, Opt. Commun. **117**, 35 (1995).

[8] A. A. Freschi and J. Frejlich, Opt. Lett. **20**, 635 (1995).

[9] P. M. Garcia, A. A. Freschi, J. Frejlich, and E. Krätzig, Appl. Phys. B: Lasers Opt. **63**, 207 (1996).

[10] V. P. Kamenov, K. H. Ringhofer, B. I. Sturman, and J. Frejlich, Phys. Rev. A **56**, R2541 (1997).

[11] E. V. Podivilov, B. I. Sturman, S. G. Odoulov, S. L. Pavlyuk, K. V. Shcherbin, V. Ya. Gayvoronsky, K. H. Ringhofer, and V. P. Kamenov, Opt. Commun. **192**, 399 (2001).

[12] E. V. Podivilov, B. I. Sturman, S. G. Odoulov, S. L. Pavlyuk, K. V. Shcherbin, V. Ya. Gayvoronsky, K. H. Ringhofer, and V. P. Kamenov, Phys. Rev. A **63**, 053805 (2001).

[13] B. I. Sturman, V. P. Kamenov, M. V. Gorkounov, and K. H. Ringhofer, Opt. Commun. **216**, 225 (2003).

[14] B. I. Sturman, A. S. Gorkounova, and K. H. Ringhofer, Eur. Phys. J. D **23**, 291 (2003).

[15] E. V. Podivilov, B. I. Sturman, and M. V. Gorkounov, JETP **98**, 896 (2004).

[16] E. V. Podivilov, B. I. Sturman, and M. Gorkounov, Ukr. J. Phys. **49**, 418 (2004).

[17] M. Gorkunov, B. Sturman, M. Luennemann, and K. Buse, Appl. Phys. B: Lasers Opt. **77**, 43 (2003).

[18] J. Frejlich, P. M. Garcia, K. H. Ringhofer, and E. Shamonina, J. Opt. Soc. Am. B **14**, 1741 (1997).

[19] K. H. Ringhofer, V. P. Kamenov, B. I. Sturman, and A. I. Chernykh, Phys. Rev. E **61**, 2029 (2000).

[20] E. V. Podivilov, B. I. Sturman, S. G. Odoulov, S. M. Pavlyuk, K. V. Shcherbin, V. Ya. Gayvoronsky, K. H. Ringhofer, and V. P. Kamenov, OSA Trends Opt. Photonics Ser. **62**, 221 (2001).

[21] N. V. Kukhtarev, V. B. Markov, S. G. Odulov, M. S. Soskin, and V. L. Vinetskii, Ferroelectrics **22**, 949 (1979).

[22] B. I. Sturman, M. Mann, J. Otten, and K. H. Ringhofer, J. Opt. Soc. Am. B **10**, 1919 (1993).

[23] A. Freschi, P. M. Garcia, and J. Frejlich, Opt. Commun. **143**, 257 (1997).

[24] M. C. Barbosa, I. de Oliveira, and J. Frejlich, Opt. Commun. **201**, 293 (2002).

[25] T. E. McClelland, D. J. Webb, B. I. Sturman, E. Shamonina, M. Mann, and K. H. Ringhofer, Opt. Commun. **131**, 315 (1996).

[26] B. I. Sturman, E. V. Podivilov, K. H. Ringhofer, E. Shamonina, V. P. Kamenov, E. Nippolainen, V. V. Prokofiev, and A. A. Kamshilin, Phys. Rev. E **60**, 3332 (1999).